# EFFECTS OF OBSTACLES ON QCM BIOSENSOR EFFICIENCY: A PARAMETRIC STUDY

**Kubíčková L.[1], Studeník O.[2], Plachá M.[3], Forinová M.[4], Isoz M.[5]**

**Abstract:** *Quartz Crystal Microbalance (QCM) biosensors are often used for the rapid detection of pathogens, for example, in drinking water. The pathogens are caught by antibodies attached to the crystal surface, leading to an increase in the attached mass and a subsequent change in the crystal resonant frequency. However, in the standard geometry configuration, most pathogens are caught in areas with limited crystal sensitivity. In our previous study, we numerically investigated the effect of geometry changes on pathogen detection efficiency. In particular, obstacles were added on the top non-detecting wall of the biosensor cell to channel the flow with pathogens. In this work, we follow up on the achieved results and conduct a parametric study focusing on tuning the previously found best obstacle layouts. With the tuned parameters, a further increase in the detection efficiency was observed.*

**Keywords: QCM biosensor, immersed boundary, lagrangian particle tracking, OpenFOAM**

## 1. Introduction

Biosensors utilizing Quartz Crystal Microbalance (QCM) technology are becoming a popular option for pathogen detection due to their small size, versatility, and fast response time (Lim et al., 2020). Pathogen detection is based on measurements of the QCM crystal resonant frequency, which changes with the amount of mass adhered to the crystal surface. To ensure pathogen adhesion, the crystal surface is coated with a polymer brush to which pathogen-specific antibodies are attached.

However, the crystal sensitivity to changes in the amount of adhered mass is not uniform across its entire surface. Typically, QCM biosensors are circular and the mass sensitivity has a radial dependence that reaches its maximum in the center and drops to almost zero near the edges (Cumpson and Seah, 1990). Hence, only a fraction of attached pathogens is actually detected and the efficiency of detection is correlated with the spatial distribution of the captured pathogens.

In our previous study (Kubíčková et al., 2025), we prepared a mathematical model of the biosensor and invcommentestigated how changes in the geometry of the biosensor flow cell affect the detection efficiency. In particular, the effect of obstacles added onto the top non-detecting wall of the cell was observed. Several different obstacle layouts were tested and the best achieved a 17 % relative increase in efficiency compared to the geometry without obstacles.

In this study, we start with the best layout and introduce various geometric modifications, including changes in obstacle length, obstacle number, or addition of perpendicular protrusions. Each change was parameterized, and the dependence of the detection efficiency on the parameters was investigated.

## 2. Mathematical model

The mathematical model of the biosensor consists of two consecutive steps. First, the flow field inside the flow cell is solved. Obstacles are added via our in-house variant of immersed boundary (IB) method, the

[1] Ing. Lucie Kubíčková: Institute of Thermomechanics, Czech Academy of Sciences (CAS), Dolejškova 1402/5; 182 00, Prague; CZ, luciekub@it.cas.cz

[2] Ing. Ondřej Studeník: Institute of Thermomechanics, CAS, Dolejškova 1402/5; 182 00, Prague; CZ

[3] Ing. Marie Plachá, Ph.D.: University of Chemistry and Technology, Prague, Technická 5; 166 28 Prague 6 – Dejvice; CZ

[4] Mgr. Michala Forinová: Institute of Physics, CAS, Na Slovance 1999/2; 182 00 Prague 8; CZ

[5] Ing. Martin Isoz, Ph.D.: Institute of Thermomechanics, CAS, Dolejškova 1402/5; 182 00, Prague; CZ

hybrid fictitious domain-immersed boundary method (Isoz et al., 2022). Second, the flow field is taken as input into a Lagrangian particle tracking method to model the movement of pathogens inside the biosensor.

**Fluid flow with obstacles**   To account for the presence of obstacles in a computational domain, the IB method uses a scalar field $\lambda$. Cells that are fully inside an obstacle have $\lambda = 1.0$ and cells that are fully outside have $\lambda = 0.0$. For cells intersected by the fluid-solid interface, the value of $\lambda$ is calculated based on the signed perpendicular distance of the cell center from the obstacle surface.

The field $\lambda$ determines the domain of effect of an IB-induced momentum source $\boldsymbol{f}_{\text{ib}}$. For steady state incompressible flow, the governing equations can be written as

$$\mathcal{M}(\boldsymbol{u}) = -\nabla\tilde{p} + \boldsymbol{f}_{\text{ib}}, \qquad \mathcal{M}(\boldsymbol{u}) = \nabla \cdot (\boldsymbol{u} \otimes \boldsymbol{u}) - \nabla \cdot \left[\nu\left(\nabla\boldsymbol{u} + \nabla\boldsymbol{u}^{\text{T}}\right)\right]$$
$$\nabla \cdot \boldsymbol{u} = 0 \qquad\qquad \boldsymbol{f}_{\text{ib}} = \text{ceil}(\lambda)\left(\mathcal{M}(\boldsymbol{u}_{\text{ib}}) + \nabla\tilde{p}\right) \qquad (1)$$

where $\tilde{p}$ is kinematic pressure, $\boldsymbol{u}$ velocity, and $\nu$ kinematic viscosity. The value of $\boldsymbol{f}_{\text{ib}}$ is calculated from the prescribed velocity values $\boldsymbol{u}_{\text{ib}}$. In cells inside obstacles, $\boldsymbol{u}_{\text{ib}} = \boldsymbol{0}$. For intersected cells, $\boldsymbol{u}_{\text{ib}}$ is reconstructed by polynomial interpolation based on the values in the free stream and the boundary condition on the obstacle surface. For more details on the IB method, see (Isoz et al., 2022).

Boundary conditions used for velocity are no-slip at walls and obstacle surface, prescribed value at the input, and zero gradient at the outlet. For pressure, the zero-gradient boundary condition is used everywhere except for the outlet where the pressure value is prescribed. Eventually, the system is discretized using the open source C++ library OpenFOAM (Weller et al., 2021) and solved using the SIMPLE algorithm with modifications for the IB method as reported in (Kubíčková and Isoz, 2023).

**Domain and obstacle geometry**   The geometry and dimensions of the computational domain are given in Fig. 1a and 1b. Obstacles were added to the top wall of the domain. The obstacles had a sphero-cylindrical shape and are shown in Fig. 1c and 1d.
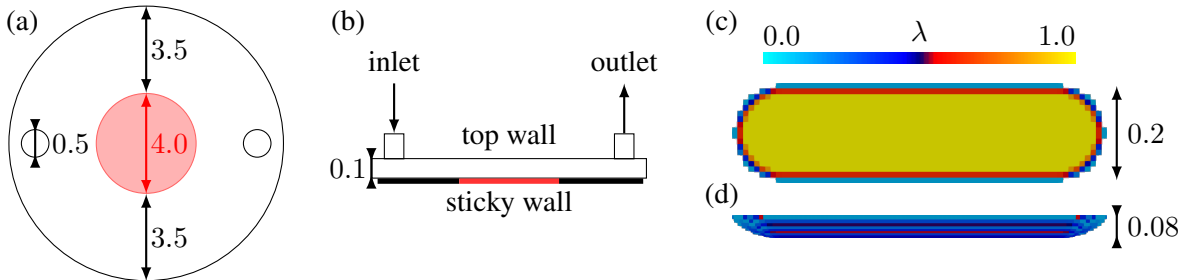


*Fig. 1: (a) Top and (b) side view on computational domain. The most sensitive region is highlighted in red. (c) Top and (d) side view on a sphero-cylindrical obstacle colored by $\lambda$ field. All dimensions are in millimeters. Based on (Scott Lynn Jr. et al., 2024) and (Kubíčková et al., 2025).*

**Particle motion**   The movement of particles was modeled using a Lagrangian tracking approach for small, spherical, and sparsely distributed particles with added Brownian motion. The model was presented by (Plachá et al., 2024). The particles movement is described by the Newton second law of motion with acting gravitational ($\boldsymbol{F}_{\text{G}}$), drag ($\boldsymbol{F}_{\text{D}}$) and Brownian force ($\boldsymbol{F}_{\text{B}}$)

$$\rho_{\text{P}}\, V_{\text{P}} \frac{\text{d}\boldsymbol{u}_{\text{P}}}{\text{d}t} = \boldsymbol{F}_{\text{D}} + \boldsymbol{F}_{\text{G}} + \boldsymbol{F}_{\text{B}}, \quad \boldsymbol{F}_{\text{D}} = 3\pi\mu\, d_{\text{P}}(\boldsymbol{u} - \boldsymbol{u}_{\text{P}}), \quad \boldsymbol{F}_{\text{B}} = \rho_{\text{P}}\, V_{\text{P}}\, \boldsymbol{G}\sqrt{\frac{\pi S_0}{\Delta t_{\text{P}}}}, \qquad (2)$$

where $V_{\text{P}}$ is particle volume, $\rho_{\text{P}}$ particle density, $d_{\text{P}}$ particle diameter and $\boldsymbol{u}_{\text{P}}$ particle velocity. The drag force formulation is based on the Stokes law for laminar flow with $\boldsymbol{u}$ being the velocity of the fluid. The Brownian force was modeled in agreement with (Li and Ahmadi, 1993) utilizing $\boldsymbol{G}$ as a vector of zero-mean independent Gaussian random numbers of unit variance and $S_0$ as the spectral intensity of Gaussian white noise. Lastly, $\Delta t_{\text{P}}$ is the integration step.

Particles enter the domain through the inlet boundary and escape through the outlet. When in contact with the sticky wall that represents the QCM crystal surface, they are captured. Upon contact with other walls, they are rebound.

**Efficiency of detection**    The Lagrangian tracking method is used to track the movement of millions of particles through the biosensor. After that the efficiency of pathogen detection is evaluated as

$$\eta = \frac{\text{particles captured in the most sensitive region}}{\text{escaped particles + all captured particles}} . \tag{3}$$

## 3.    Numerical experiments

Previously, the described mathematical model was used to calculate performance indicators for biosensor without obstacles and biosensors with obstacles in various layouts. Details about the study are given in (Kubíčková et al., 2025). The best found obstacles layout is given in Fig. 2b. Compared to the biosensor without obstacles shown in Fig. 2a, the efficiency increased from 3.73 % to 4.38 % which is a relative increase of 17 %.
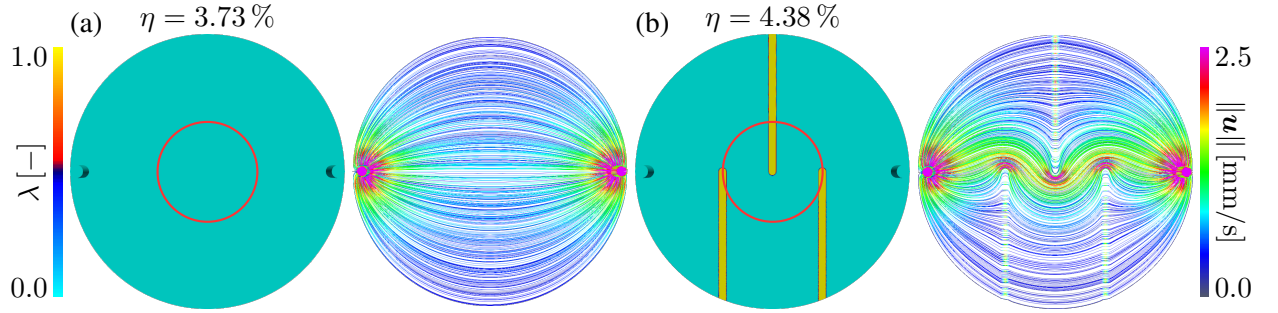


*Fig. 2: Summary of results for (a) biosensor without obstacles and (b) biosensor with the best obstacle layout from our previous study presented in (Kubíčková et al., 2025).*

In this study, the effects of geometric modifications of the best layout were investigated. Three different modifications with parametrization are shown in the top of Fig. 3. In the bottom of Fig. 3, the dependency of the detection efficiency on the parameters is given. The highest detection efficiency was given in the modification with five obstacles for the parameter value $\Delta y = -2.0 \, \text{mm}$ where $\eta = 5.22 \, \%$. Compared to the configuration without obstacles, the relative increase in efficiency was 39.7 %.
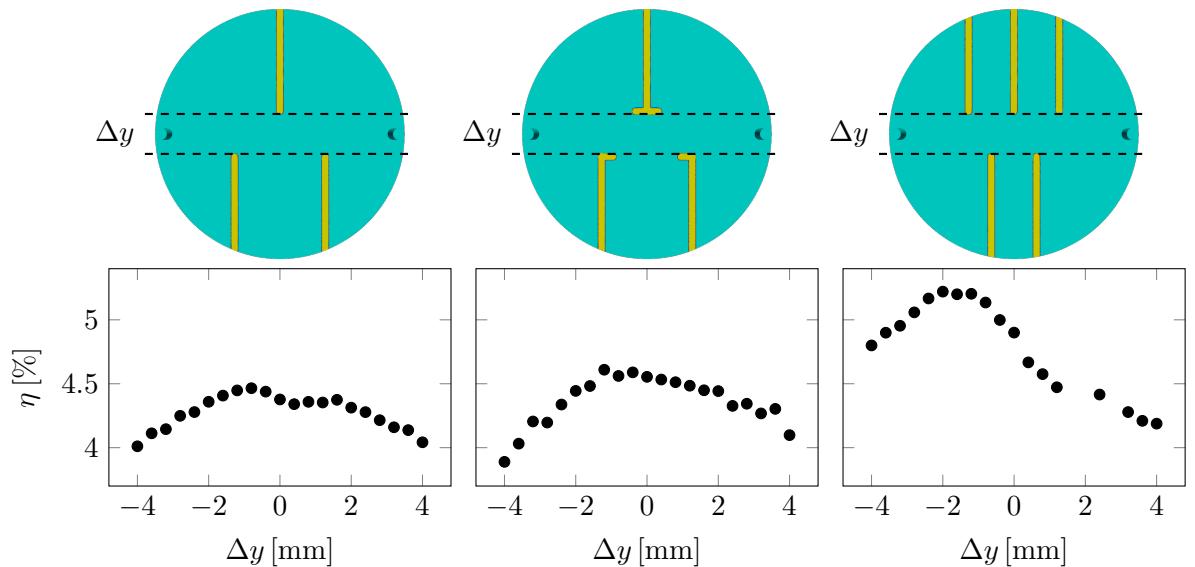


*Fig. 3: Effects of geometric modifications of the detection efficiency. The modifications with parametrization are in the top. The dependency of the detection efficiency with respect to the parameters is in the bottom.*

## 4.    Conclusions

In this contribution, we focused on the efficiency of pathogen detection of a QCM biosensor. In particular, the effect of obstacles added onto the top non-detecting wall of the biosensor flow cell was investigated.

Previously, we had developed a mathematical model of the biosensor and found an obstacle layout that led to higher efficiency. In the present work, this layout was taken as a baseline, and geometric modifications to the layout were introduced and parametrized. The dependency of the detection efficiency on the parameters was studied. The greatest increase in efficiency was observed for a modification with 5 obstacles where the efficiency increased by $19.3\,\%$ relative to the baseline layout and by $39.7\,\%$ relative the flow cell without obstacles. Based on this parametric study, it can be expected that further modifications of obstacle layouts may lead to even higher efficiency. Hence, our future goal is to perform a topology optimization of the layout.

## Acknowledgments

## References

Cumpson, P. and Seah, M. (1990) The quartz crystal microbalance; radial/polar dependence of mass sensitivity both on and off the electrodes. *Measurement Science and Technology*, 1, pp. 544.

Isoz, M., Šourek, M. K., Studeník, O., and Kočí, P. (2022) Hybrid fictitious domain-immersed boundary solver coupled with discrete element method for simulations of flows laden with arbitrarily-shaped particles. *Computers & Fluids*, 244, pp. 105538.

Kubíčková, L. and Isoz, M. (2023) On Reynolds-averaged turbulence modeling with immersed boundary method. In Šimurda, D. and Bodnár, T., eds, *Proceedings of Topical Problems of Fluid Mechanics 2023*. IT CAS, pp. 104–111.

Kubíčková, L., Studeník, O., Plachá, M., and Isoz, M. (2025) Improving QCM biosensor efficiency by flow cell modification. In Šimurda, D. and Bodnár, T., eds, *Proceedings of Topical Problems of Fluid Mechanics 2025*. IT CAS, pp. 159–166.

Li, A. and Ahmadi, G. (1993) Computer simulation of deposition of aerosols in a turbulent channel flow with rough walls. *Aerosol Science and Technology*, 18, pp. 11–24.

Lim, H., Saha, T., Tey, B., Tan, W., and Ooi, C. (2020) Quartz crystal microbalance-based biosensors as rapid diagnostic devices for infectious diseases. *Biosensors and Bioelectronics*, 168, pp. 112513.

Plachá, M., Isoz, M., Kočí, P., Jones, M., Svoboda, M., Eastwood, D., and York, A. (2024) Particle accumulation model in 3D reconstructed wall of a catalytic filter validated with time-resolved X-ray tomography. *Fuel*, 356, pp. 129603.

Scott Lynn Jr., N., Forinová, M., Spasovová, M., and Vaisocherová-Lísalová, H. (2024) Radial flow enhances QCM biosensor sensitivity. *Sensors and Actuators: B. Chemical*, 401, pp. 134949.

Weller, H., Greenshields, C., and et al., W. B. (2021) The OpenFOAM foundation.